References and Notes

1. G. L. Nelms *et al.*, *Can. J. Res.* **44**, 1419 (1966).
2. With the magnetic-dipole moment μ of about 10^{-20} erg/gauss, we expect approximate equality of the concentrations, of a particular species, with dipoles parallel and antiparallel to the local magnetic field, both equalling $N/2$—half the total concentration. For the particles indicated by the Alouette signal, the probability of reemission, equal to the probability of absorption, in terms of the Einstein coefficient for stimulated emission, is

$$W = [2\pi(\mu^2/3)/\hbar^2 c](dI/d\nu) = 2 \times 10^4\,(dI/d\nu)\ \text{sec}^{-1}$$

where $dI/d\nu$ is the energy flux from the sounder-transmitter per unit frequency interval. The average radiated power, 300 watts, is spread over a bandwidth of about 30 kcs. If one neglects absorption between the satellite and a point at distance R, the energy flux at R is

$$dI/d\nu = 10^5/4\pi R^2\ [\text{erg/cm}^2\ \text{sec (cy/sec)}]$$

We neglect the angular dependence and assume that the power reflected by a population of N magnetic dipoles per cubic centimeter, given by

$$P(R) = W\ (N/2)\ h\nu = 0.5 \times 10^9\,(N/2)\,h\nu/4\pi R^2\ (\text{erg/cm}^3\ \text{sec})$$

is radiated isotropically. It is assumed that the radiated power density is approximately constant over the line width of the effective radicals. The intensity of the signal arriving at the satellite at time t, measured from the time at which the 100-μsec transmitter pulse begins, is given by

$$S(t) = \int [P(R)/4\pi R^2]\,dV\ (\text{erg/cm}^2\ \text{sec})$$

where the integral is taken over the volume of origin of reemitted radiation reaching the satellite at time t. This volume is a spherical shell centered on the satellite. For a pulse of 100 μsec, the inner surface of the shell has radius $R_1 = c(t - 100)/2$, and the outer surface has radius $R_2 = ct/2$, where t is measured in microseconds. By integration over the spherical angular coordinates and use of $\nu = 10^6$ cy/sec, it follows that

$$S(t) = \int_{R_1}^{R_2} P\,dR = 1.5 \cdot 10^{-13}\,N \int_{R_1}^{R_2} dR/R^2$$

If the signal is to be detected at the satellite, $S(t)$ must be greater than the threshold of the receiver, that is, $S(t) \geq 3 \times 10^{-15}$ erg/cm^2 sec. Furthermore the signal must be at least 100-μsec long, that is, $t = 202$ μsec. For the minimum value of detectable signal, therefore,

$$\int_{R_1}^{R_2} dR/R^2 = 6 \times 10^{-7}\ \text{and}\ N \geq 3 \cdot 10^4\ \text{cm}^{-3}$$

3. L. Marshall and W. F. Libby, *Nature* **214**, 126 (1967).
4. See, for example, D. J. E. Ingram, *Free Radicals* (Butterworths, London, 1958), pp. 218–22; J. Sheridan, *Ann. Rept. Progr. Chem. Chem. Soc. London* **44**, 7 (1957); ———, *ibid.* **60**, 160 (1963).
5. C. Moore, *U.S. Nat. Bur. Std. Circular 467*; L. Wiese, M. W. Smith, B. M. Glennon, "Atomic transition probabilities," in *NSRDS-NBS 4*, vol. 1.
6. R. Beringer and J. G. Castle, *Phys. Rev.* **78**, 581 (1950); R. Beringer, E. B. Rawson, A. F. Henry, *ibid.* **94**, 343 (1954); C. C. Lin and M. Mizushima, *ibid.* **100**, 1726 (1955); H. E. Radford, *ibid.* **122**, 114 (1961).
7. Ne III, IV, and V also show the same Landé g values, but the abundance of neon in Earth's atmosphere is marginally small for detection with this receiver.
8. R. W. Zimmerer, thesis, University of Colorado (1960).
9. We believe the 180° magnetic-dipole reflections that we report to be exactly analogous with the 180° resonant electric-dipole plasma reflections routinely observed from the ionosphere by ground-based stations.
10. Work aided by NASA grant 237-62, contract 249-62. We thank G. L. Nelms, T. R. Hartz (both of the Canadian Defense Research Telecommunications Establishment), and W. Calvert (U.S. National Bureau of Standards) for advice and information regarding the Alouette instrument; C. Sonett, L. Colin, and K. L. Chan (Ames Research Center) for lending the south polar records of Alouette II; D. Stork (University of California, Los Angeles) for use of film-measuring equipment; and M. Mizushima (University of Colorado) for discussions of the magnetic properties of molecular oxygen.

* Aided by USAF Chemical Directorate grant AF-AFOSR-245-65.

† Supported by AEC contract AT (11-1)-1537.

16 May 1967

Geostrophic Transport Through the Drake Passage

Abstract. *Geostrophic velocity and transport of water in the Drake Passage relative to a newly defined zero reference layer indicate that the circumpolar current is basically north of 59°S, with its axis north 57°S, and that the total volume transport exceeds 200 × 10⁶ cubic meters per second. The calculated geostrophic velocities are consistent with results of descriptive water-structure studies.*

Estimates of the total volume transport through the Drake Passage vary from 0 (*1*) to 165 × 10^6 m^3/sec (*2*). The uncertainty arises from a lack of direct current measurements and an inability to define a satisfactory reference layer. The reference layer is needed to convert relative geostrophic velocities into absolute values. For this purpose, the level of no motion or the zero reference layer is generally used. It can be found by various methods (*3*).

In general, velocity decreases with depth; therefore, any deep isobaric surface would suffice as a zero reference layer for the determination of surface currents. However, the depth of the zero reference layer becomes critical for calculations of deep currents and total volume transport.

Table 1 summarizes the past estimates of the total volume transport through the Drake Passage. The transport values vary with changes of the reference layer, even though, in many cases, the same hydrographic data are used.

The zero reference layer in the southern Drake Passage (*4*) is used to determine the mean density of overlying water. The reference layer may then be extended northward by use of the equivalent-barotropic assumption (*5*). This assumption has yielded meaningful results in stratified water (*5*) and may be of use in water of a homogeneous nature such as that found in the Antarctic Ocean. The assumption was applied to the Drake Passage by Ostapoff (*1, 6*); however, the initial zero reference layer was found by extrapolation of Defant's Atlantic Ocean reference layer (*7*) into the Drake Passage. Ostapoff's resulting velocities show a westward-flowing deep and bottom current. This calculation does not agree with the descriptive analysis of the hydrographic data which indicates that the bottom flow of the northern Drake Passage is rapid and toward the east, and that no zero reference layer exists within the water column of the northern Drake Passage (*4, 8*).

The hydrographic stations for which geostrophic calculations were performed are plotted in Fig. 1. The calculated velocities are perpendicular to the

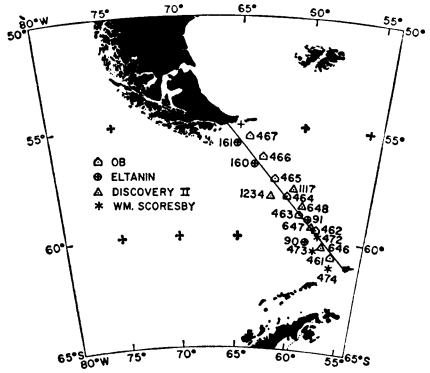

Fig. 1. Hydrographic stations used in geostrophic calculations.

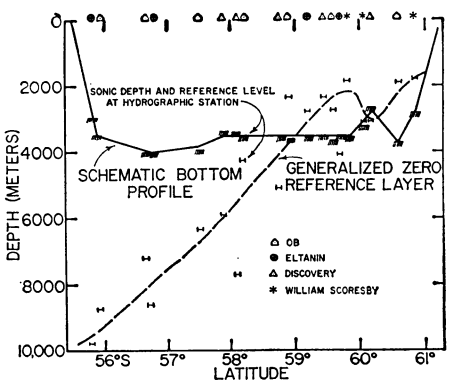

Fig. 2. Depth of zero reference layer in the Drake Passage.

indicated line; therefore, they represent the northeast component of the total geostrophic velocity. Based on the potential relationship between temperature and salinity in the Drake Passage, the zero reference layer at *Eltanin* Station 91 is 2750 m (*4*, fig. 1). The mean density of the water column above the zero reference layer is 27.77.

By use of a mean density of 27.77, the depth of the zero reference layer was found for all stations shown in Fig. 1. Figure 2 is a plot of the depth of the average zero reference layer. The reference layer descends from a minimum of 1800 m in the south to over 9000 m in the northern Drake Passage. The depth of the zero reference layer probably has a time variation. The dashed line shown in Fig. 2 represents an average condition. Extrapolation below the sea floor was necessary to calculate velocities relative to this reference layer. Since the water is fairly homogeneous in the Antarctic Ocean and there is only slight attenuation of currents with depth (*8*), extrapolation techniques are probably valid.

There are four sets of data: (i) *Ob* stations 461–467, (ii) *Eltanin* stations 90–91 and 160–161, (iii) *Discovery* station pairs 646–647, 647–648, and 1117–1234, and (iv) *William Scoresby* station pairs 472–473 and 473–474. The calculated velocities from the *Ob* and *Eltanin* data are shown in Fig. 3, and the *Discovery* and *William Scoresby* results are shown in Fig. 4. The geostrophic velocities are represented in box form since the values are average velocities at standard levels between the two hydrographic stations.

Table 1. Estimates of the volume transport through the Drake Passage by various authors.

Author	Data	Season	Reference layer (m)	Method of finding reference	Total volume transport 10^6 m^3/sec)
1933 Clowes (*12*)	*Discovery*	Summer	3500	DIS*	110 (above 3500 m)
1942 Sverdrup (*13*)	Composite: mostly *Discovery* and *William Scoresby*	Composite	3000	DIS	90
1959 Kort (*2*)	*Ob*	Winter	3000	DIS	134
				Bottom	165
1960 Ostapoff (*1*)	*Discovery*	Summer	Variable	Defant's method with equivalent-barotropic assumption	0
1961 Ostapoff (*6*)	*Discovery*	Summer	Variable	Same as above	0
			2000	DIS	33
			3000	DIS	85
	Ob	Winter	Variable	Defant's method with equivalent-barotropic assumption	9
			2000	DIS	34
			3000	DIS	86
1962 Yeskin (*10*)	Composite	Summer	3500	DIS	150
		Winter			123
1965 Vorob'yev and Gindysh (*14*)	Composite	Summer	Variable	Defant's method	120
		Winter	Variable	Defant's method	91
1967 Gordon (*15*)	*Ob*	Winter	Variable	T/S† relation, with equivalent-barotropic assumption	218

* DIS, deep isobaric surfaces. † T S, temperature/salinity.

The *Ob* section is most complete in that it consists of evenly spaced stations across the Drake Passage. Currents above 10 cm/sec are found north of 59°S. To the south of this latitude, velocities are low (less than 5 cm/sec at all levels) and a weak westward flow occurs between 59° and 60°S. Velocities of 30 to 31 cm/sec are found between stations 466 and 467 from the surface to 2500 m, with a bottom velocity of 21 cm/sec. This observation is consistent with photographs which indicate the presence of large bottom currents in the northern Drake Passage (*9*). South of station 466, the deep and bottom currents are of lower magnitude, usually below 5 cm/sec. The axis of the circumpolar current is north of 57°S.

The two *Eltanin* station pairs in Fig. 3 indicate velocities similar to the *Ob*

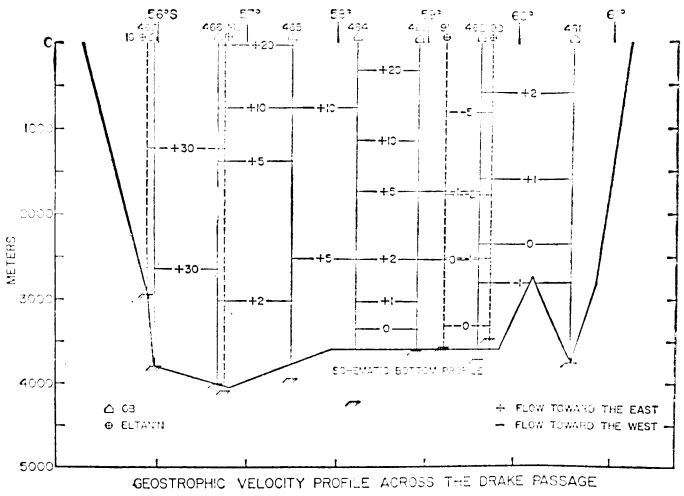

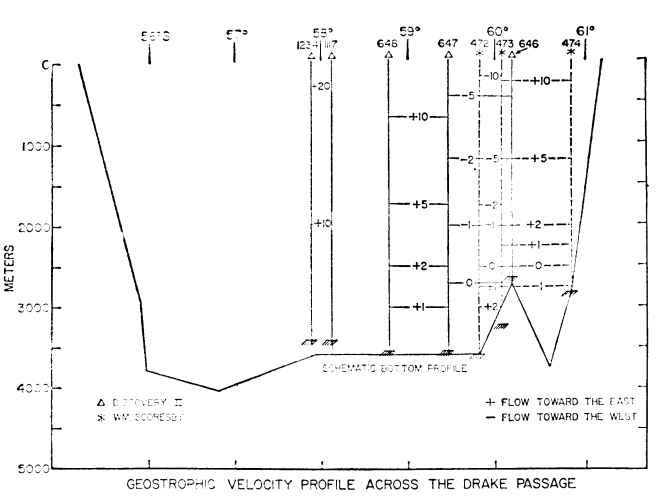

Fig. 3 (left). Geostrophic velocities (centimeters per second) in the Drake Passage calculated from *Ob* and *Eltanin* hydrographic stations. The two *Eltanin* station pairs are represented by dashed lines. Fig. 4 (right). Geostrophic velocities (centimeters per second) in the Drake Passage calculated from *Discovery* and *William Scoresby* hydrographic stations. The two *William Scoresby* stations are represented by dashed lines.

results. The westward flow between stations 90–91 is slightly more intense and deep-reaching than that of the *Ob*.

The *Discovery* and *William Scoresby* profiles suggest that currents in the southern Drake Passage are slightly more active than those found by the *Ob*, though the directions are similar. This may represent a seasonal change, since the *Ob* section was taken in early winter and the *Discovery* and *William Scoresby* sections were taken under summer conditions. The *Eltanin* 90–91 station pair which represents summer conditions agrees more closely with the *Discovery* 646–647 stations pairs. Table 1 indicates a more active summer circulation. Yeskin finds the maximum transport occurring during March and April (*10*).

The geostrophic results indicate that the velocity field of the Drake Passage may be considered to have two parts: a northern part (north of 59°S) with moderate easterly currents extending to the bottom, and a southern part with lower velocities and westerly currents between 59° and 60°S.

The total volume transport determined from the *Ob* profile is 218 × 10^6 m^3/sec. This large value results from the generally deep-reaching effects of the axis of the circumpolar current. More than one half of this immense transport is accomplished between *Ob* stations 466 and 467, which are slightly over 80 km apart. It appears that more water passes between approximately 56° and 57°S in the Drake Passage than is carried by the Gulf Stream.

The flow south of 55°S is somewhat dependent on the quantity of water flowing through the Drake Passage (*11*). The circumpolar current, after transversing the Drake Passage, turns northward to enter the Atlantic Ocean to the west of South Georgia. The water of the eastern and southern Scotia Sea, though at the same latitude as the Drake Passage, is derived from the Weddell Sea. The line separating the waters from the Weddell Sea and Pacific Ocean is called the Bellingshausen Front. It is well defined throughout the deep and bottom water and is situated in a zone of instability in the surface water (*8*). No doubt the positioning of the Bellingshausen Front and the northward penetration of the Weddell water are dependent on the Drake Passage transport.

The results of this study are consistent with the qualitative understanding of the flow through the Drake Passage gained in earlier descriptive studies (*4, 8*). This consistence supports the validity of these findings. Direct current measurements would be needed in the Drake Passage to further test these results. Since transient motion is significant in the Antarctic Ocean (*8*), these measurements must be made over a time interval long enough to determine the geostrophic component.

ARNOLD L. GORDON
Lamont Geological Observatory of Columbia University, Palisades, New York

References and Notes

1. F. Ostapoff, *J. Geophys. Res.* **65**, 2861 (1960).
2. V. G. Kort, *Int. Oceanog. Cong., Preprints*, (AAAS, Washington, D.C., 1959), pp. 434–435.
3. L. M. Fomin, *The Dynamic Method in Oceanography* (Elsevier, Amsterdam 1964), pp. 1–212.
4. A. L. Gordon, *Deep-Sea Res.* **13**, 1125 (1966).
5. G. Neumann, *Deut. Hydrog. Z.* **9**, 66 (1956).
6. F. Ostapoff, *Deep-Sea Res.* **8**, 111 (1961).
7. A. Defant, *Physical Oceanography* (Pergamon Press, New York, 1961), vol. 1, pp. 1–729.
8. A. L. Gordon, *Amer. Geog. Soc. Antarctic Map Folio Series 6* (1967).
9. B. C. Heezen and C. D. Hollister, *Marine Geol.* **1**, 141 (1964).
10. L. I. Yeskin, *Tr. Sov. Antarkt. Eksp.* **20** (1962).
11. H. Stommel, *Deep-Sea Res.* **4**, 149 (1957).
12. A. J. Clowes, *Nature* **131**, 189 (1933).
13. H. V. Sverdrup, H. W. Johnson, R. H. Fleming, *The Oceans* (Prentice-Hall, New Jersey, 1942), p. 1087.
14. V. N. Vorob'yev and B. V. Gindysh, *Tr. Sov. Antarkt. Eksp.* **23** (AGU translation **5**), 425 (1965).
15. Supported by grant GA-305 from the NSF Office of Antarctic Programs. Lamont Geological Observatory Contribution No. 1066.

10 March 1967; revised 24 April 1967

Amazon River: Environmental Factors That Control Its Dissolved and Suspended Load

Abstract. *Analytical results of sampling during both wet and dry seasons along the Amazon River, at its mouth, and from 16 tributaries reveal that the physical weathering dominant in the Andean mountainous environment controls both the overall composition of the suspended solids discharged by the Amazon and the amount of dissolved salts and suspended solids discharged.*

The purpose of this study was to determine the factors that control erosion in the Amazon River system. The amount and composition of suspended solids and the amount of dissolved salts carried by this system are evaluated. Analysis of the composition of the dissolved salts will be reported upon completion.

The Amazon River basin was selected as the area for the present study because (i) the influence of man on its properties is negligible; (ii) the effects of local natural anomalies are minimized by the large area of the drainage basin; and (iii) the series of 16 large tributaries that drain the Amazon's wide range of geologic and climatic source areas make possible the sampling of the material before it is mixed with the materials from other tributaries, thereby permitting the testing of the hypothesized controlling factors.

Periodic (monthly to semiannual) sampling of the suspended solids, bottom sediments, and water, and the measurement of salinity, temperature, and *p*H were accomplished throughout the seasonal cycle in these 16 tributaries (accounting for more than 90 percent of tributary discharge into the Amazon River) and along the Amazon. The *in situ* conductivities were taken as a measure of the concentration of dissolved salts.

Suspended solids were removed from each of 74 samples of water (20 liters each) in the field, mainly by pressure molecular filtration (size of pores, 0.45 μ), and the material was stored in a small amount of river water with Hutner's (*1*) volatile organic preservative (a mixture of *o*-cholorobenzene, *n*-butyl chloride, and 1,2-dichloroethane) to prevent decay by microbes and alteration of the distribution of the particles according to size.

Fifty samples of the suspended material were analyzed by x-ray diffraction for mineral composition after separation, by size, into fractions (< 2 μ, 2 to 20 μ, and > 20 μ) and removal of organic material and iron oxide coatings, according to procedures published elsewhere (*2*). Analytical results were considered in connection with the environmental factors of geology, elevation, climate, and vegetation. As the possible controlling factors, nine parameters related to these four environmental factors were measured for each tributary basin from appropriate maps and data: (i) areal percentage of "calcic" rocks (limestone, dolomite, and volcanic rocks other than rhyolite); (ii) areal percentage of igneous and metamorphic rocks (mainly Precambrian shield areas of acid- to intermediate-type rocks); (iii) areal percentage of continental sedimentary rocks; (iv) areal percentage of marine sedimentary rocks, excluding "calcic" rocks; (v) areal percentage of "calcic" rocks in the upper third of each tributary basin; (vi) mean elevation (using 13 elevation intervals) above the mouth (base level) of the tributary; (vii) mean tem-